

Supporting Information for

Selective Anticancer Materials by Self-Assembly of Synthetic Amphiphiles Based on *N*- Acetylneuraminic Acid

*Jiwon Hwang,^[a] Ye Rim Kim,^[a] Jung Yeon Park,^[a] Woo Hyun Nam,^[a] Jehan Kim,^[b] Jinhan
Cho,^[c] Yongju Kim*^[a]*

[a] KU-KIST Graduate School of Converging Science and Technology, Department of Integrative Energy Engineering, Korea University, Seoul, 02841, Republic of Korea
E-mail: yongjukim@korea.ac.kr

[b] Pohang Accelerator Laboratory, Postech, Gyeongbuk, 790-784, Republic of Korea

[c] KU-KIST Graduate School of Converging Science and Technology, Department of Chemical and Biological Engineering, Korea University, 145 Anam-ro, Seongbuk-gu, Seoul, 02841
Republic of Korea

Keywords: supramolecular materials, anticancer materials, sialic acid, *N*-acetylneuraminic acid, Neu5Ac, active targeting cancer therapy, reactive oxygen species

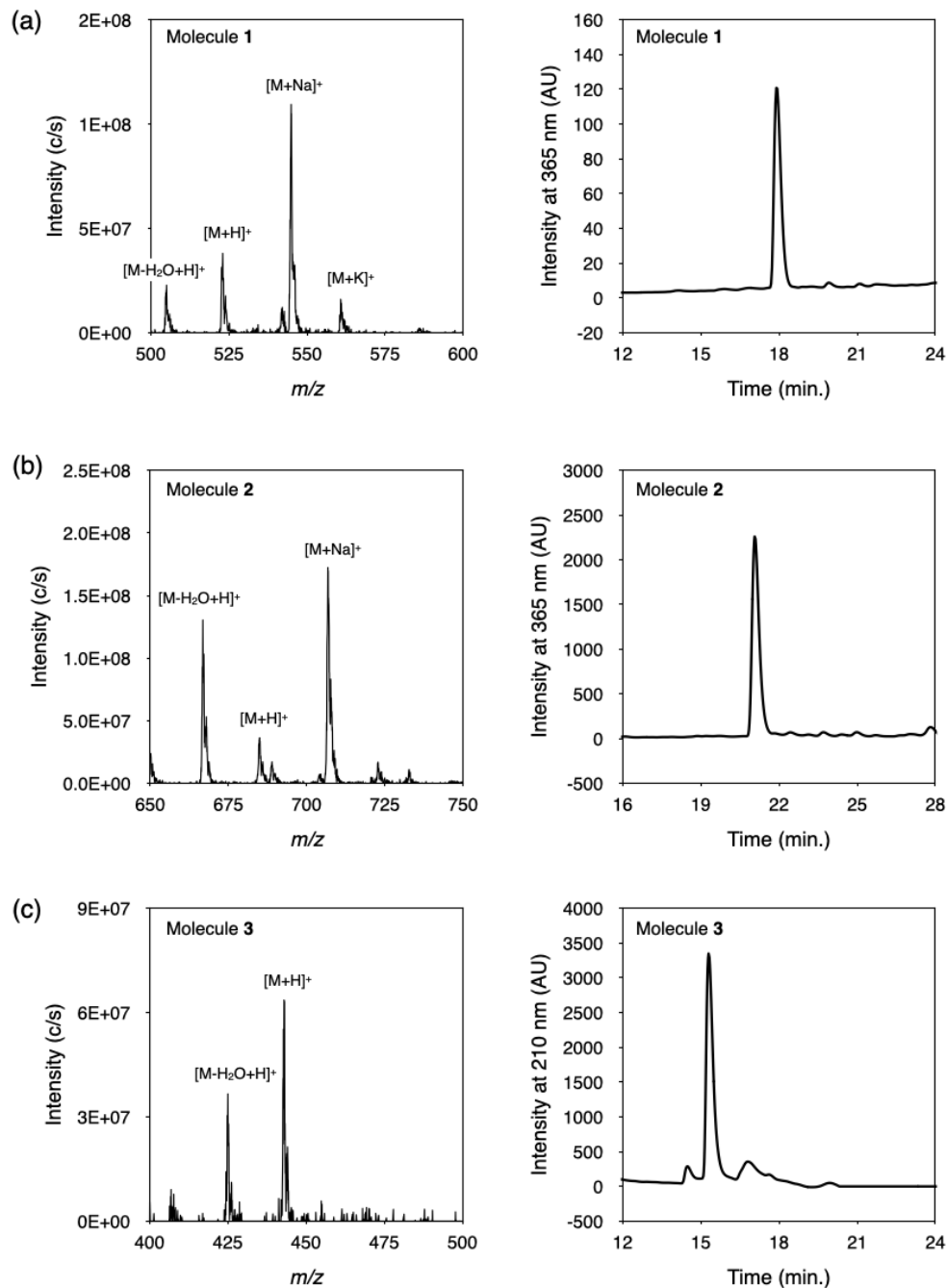
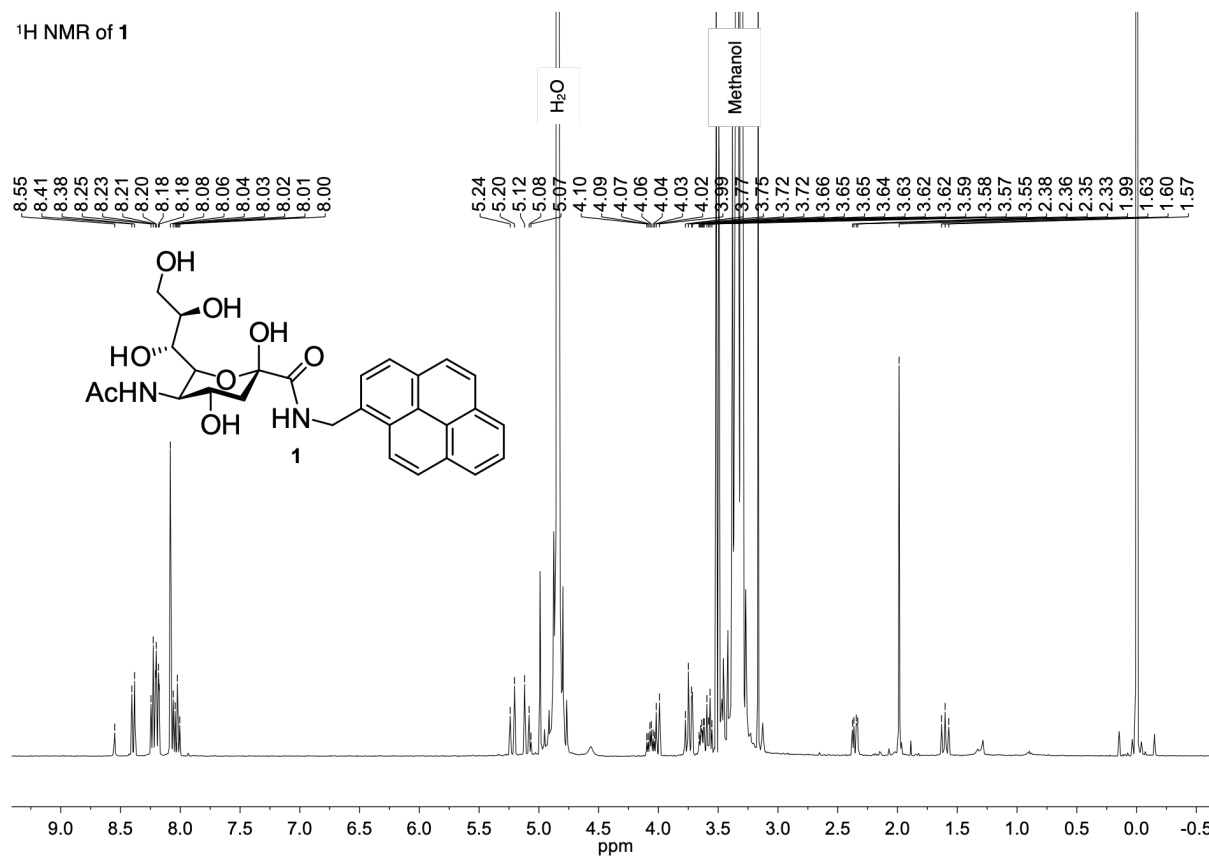


Figure S1. (a) Molecular mass and analytic HPLC spectrum of **1** ($[M + H]^+$ calcd for $C_{28}H_{31}N_2O_8$, 523.21; found, 523.0). (b) Molecular mass and analytic HPLC spectrum of **2** ($[M + H]^+$ calcd for $C_{35}H_{45}N_2O_{12}$, 685.30; found, 684.9). (c) Molecular mass and analytic HPLC spectrum of **3** ($[M + H]^+$ calcd for $C_{21}H_{35}N_2O_8$, 443.24; found, 443.0). Molecular mass was measured in 70 % CH_3CN in water with 0.1% TFA by mass spectrometer. HPLC was analyzed in H_2O/ACN 95:5 \rightarrow 0:100 condition for 30 minutes with flow rate of 0.65 ml/min.

¹H NMR of 1



¹³C NMR of 1

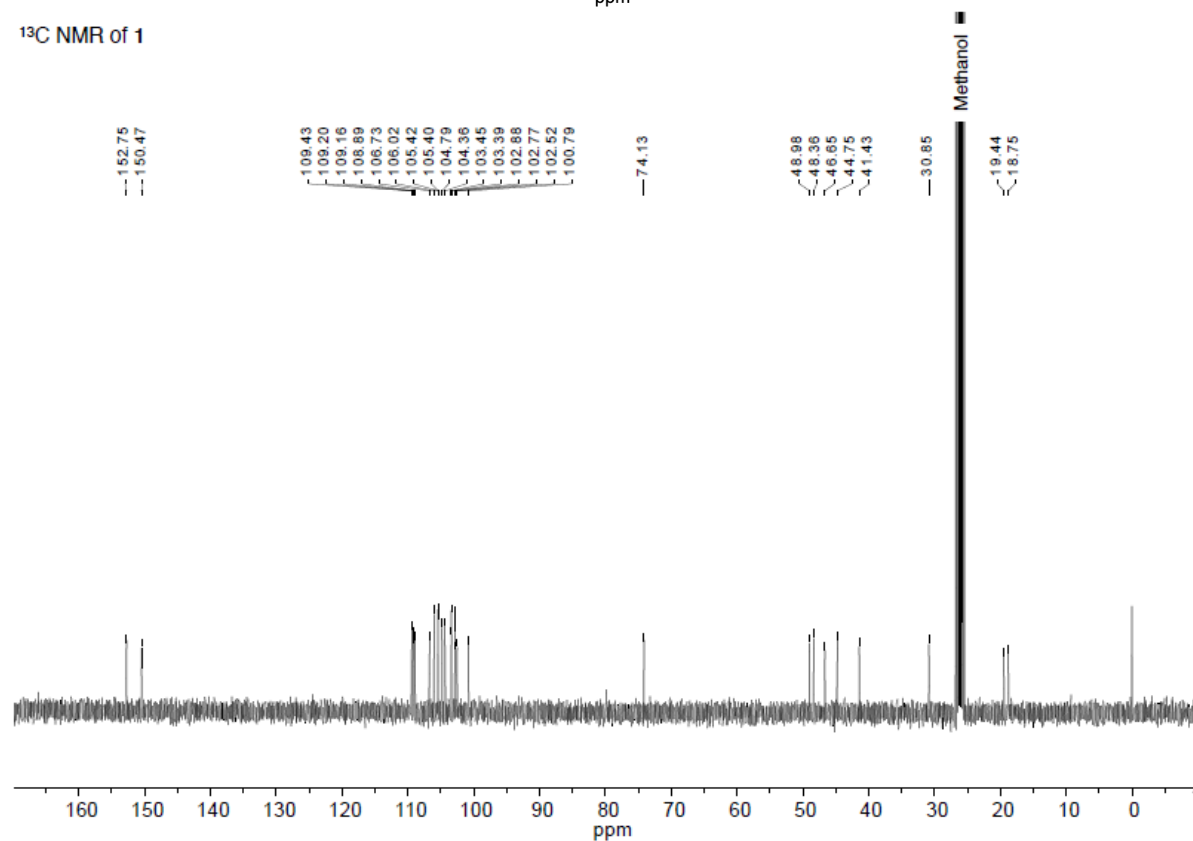


Figure S2. ¹H and ¹³C NMR of molecule 1.

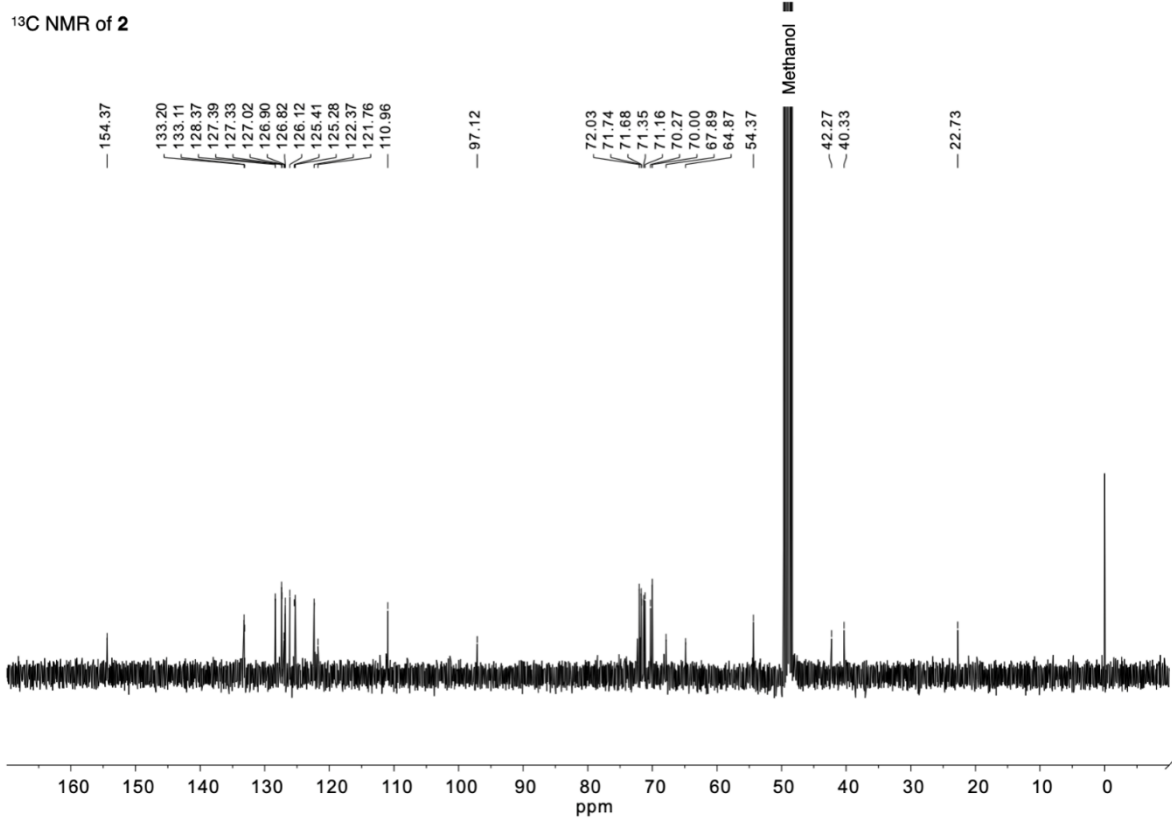
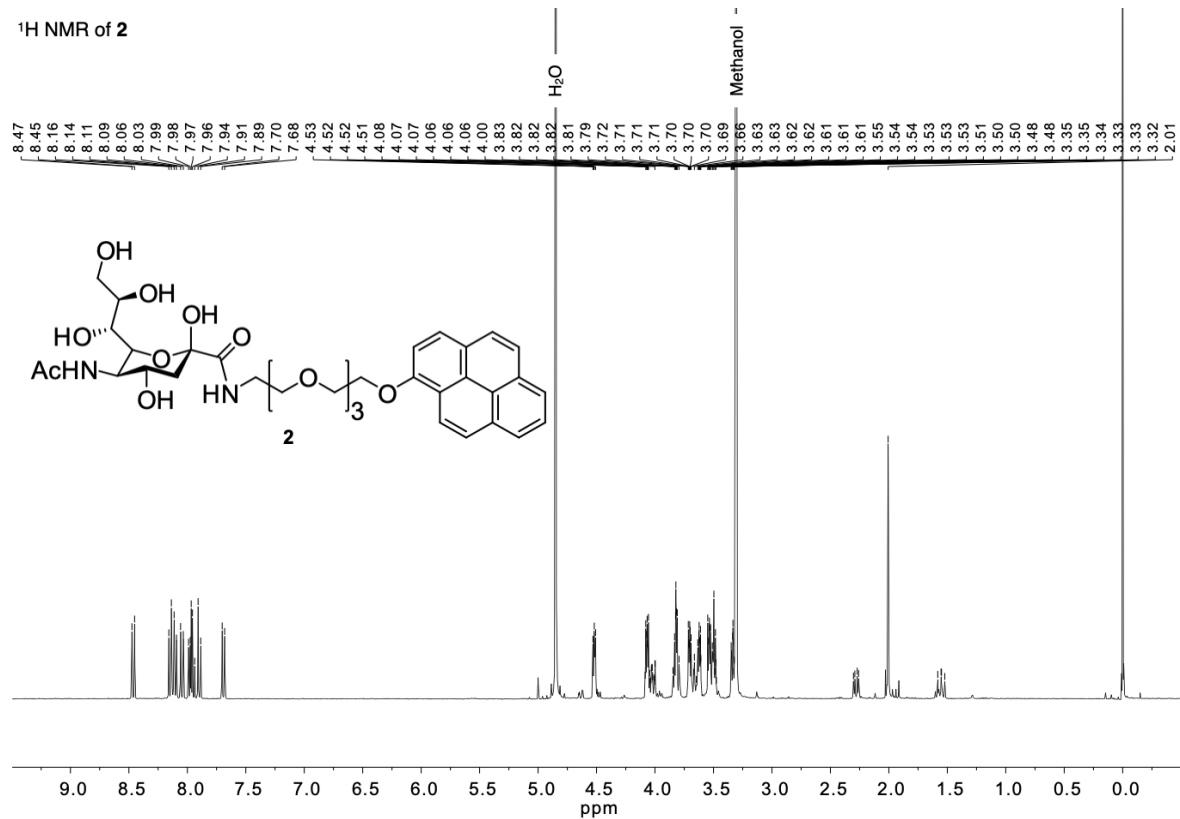
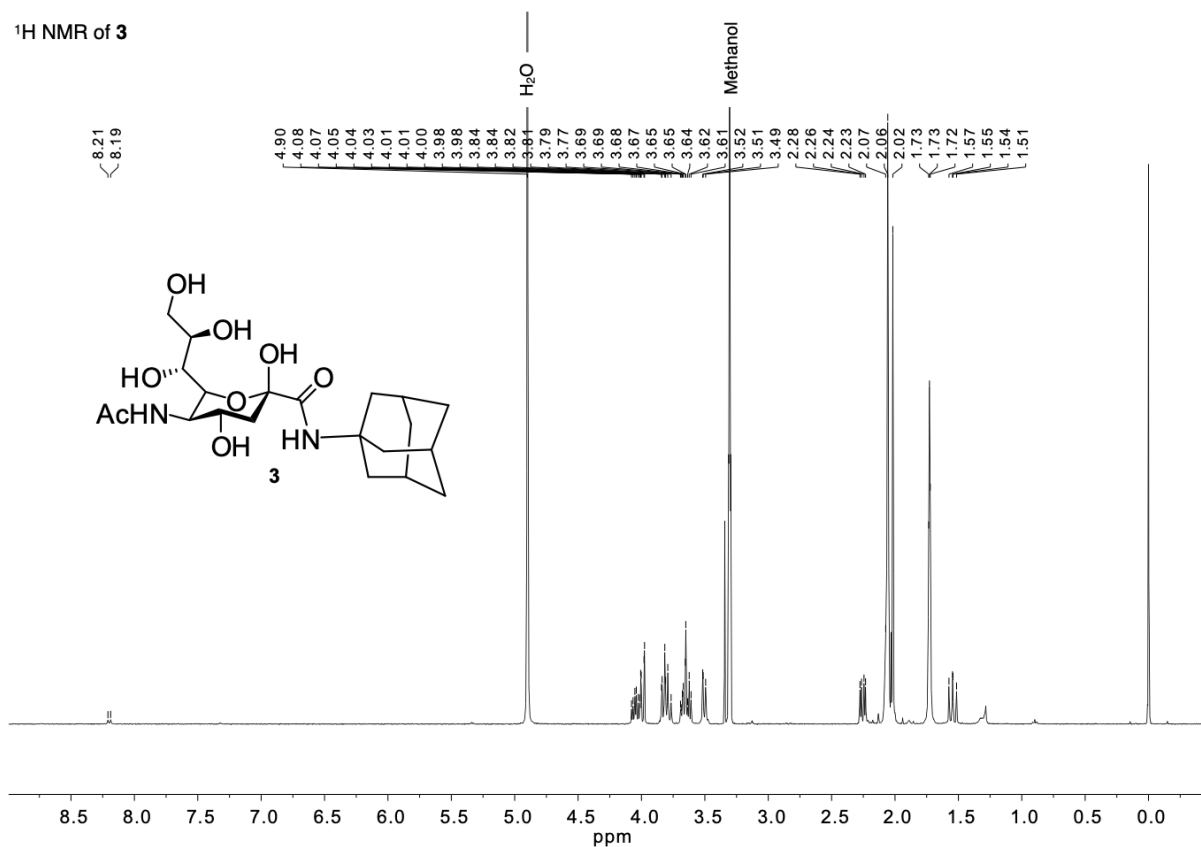


Figure S3. ¹H and ¹³C NMR of molecule 2.

¹H NMR of **3**



¹³C NMR of **3**

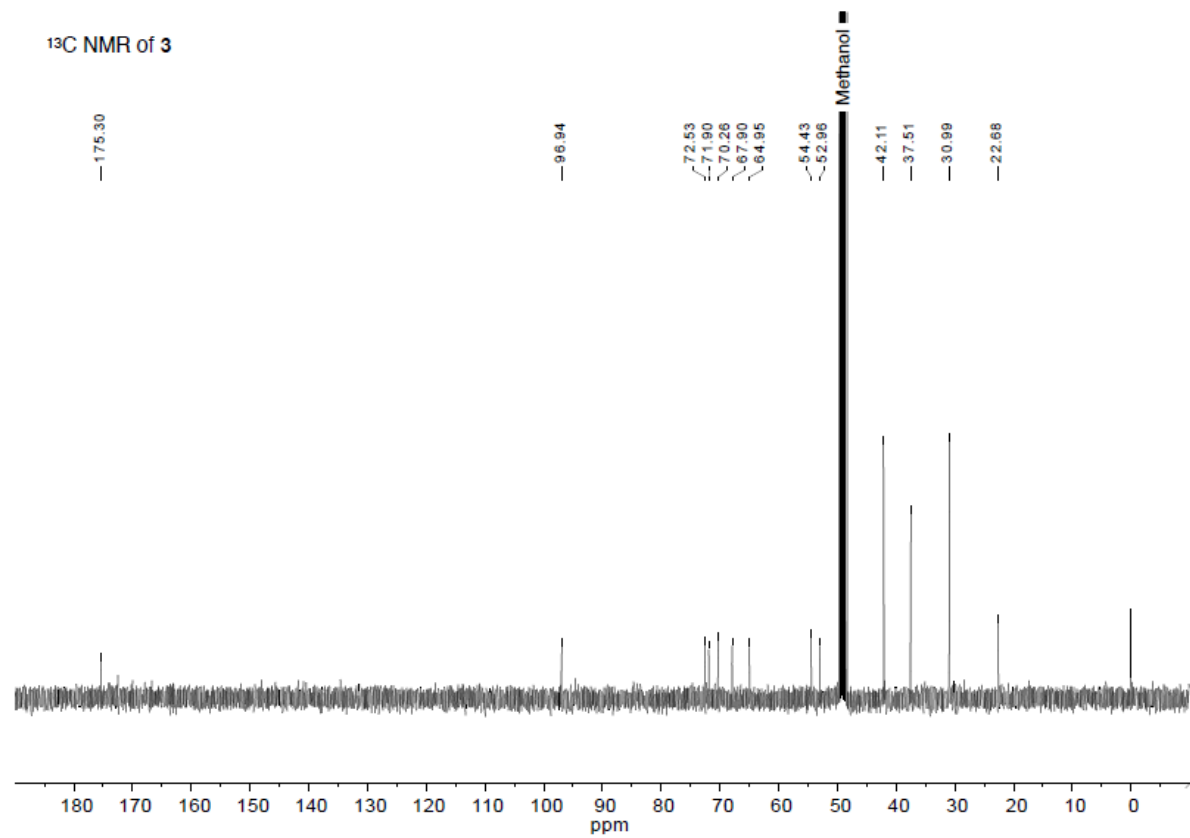


Figure S4. ¹H and ¹³C NMR of molecule **3**.

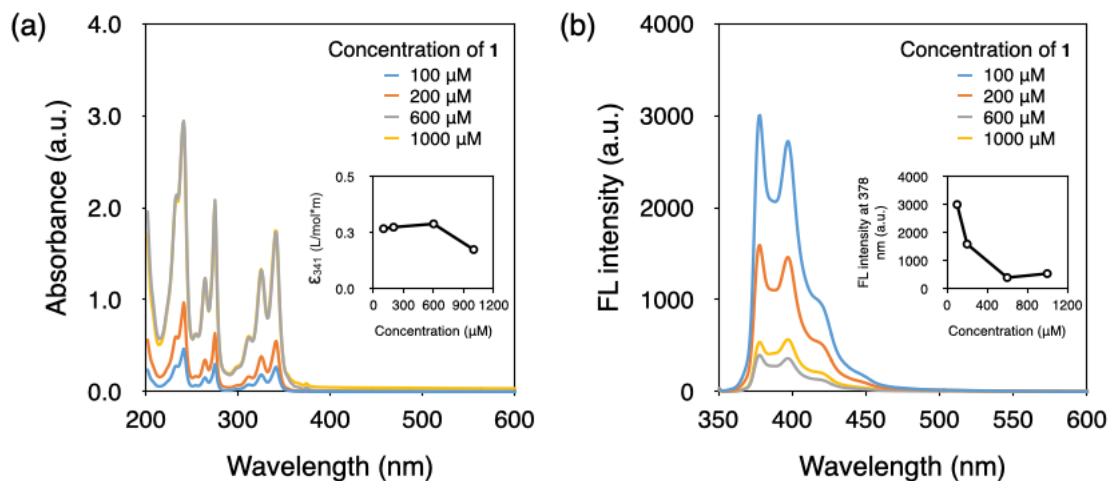


Figure S5. (a) Absorption and (b) emission spectra of molecule **1** at different concentrations (insets are the absorption coefficient and fluorescence intensity of **1** at 341 nm and 378 nm, respectively).

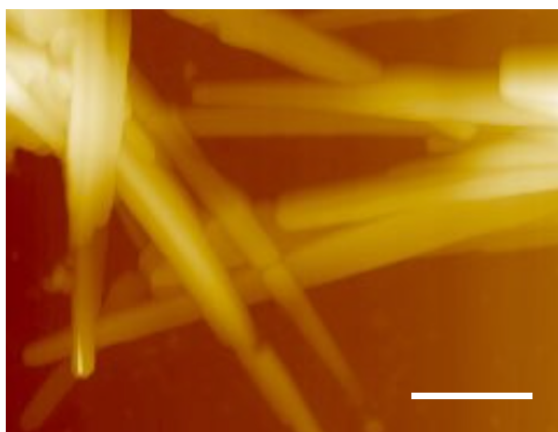


Figure S6. Atomic force microscopy image of amphiphile **1** (200 μM) in aqueous solution (scale bar, 1 μm).

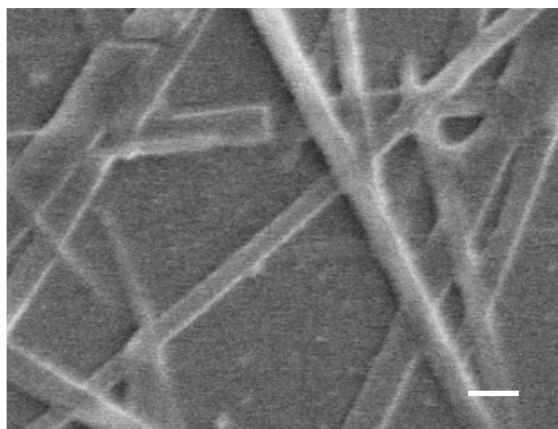


Figure S7. Scanning electron microscopy image of amphiphile **1** (200 μM) in aqueous solution (scale bar, 500 nm).

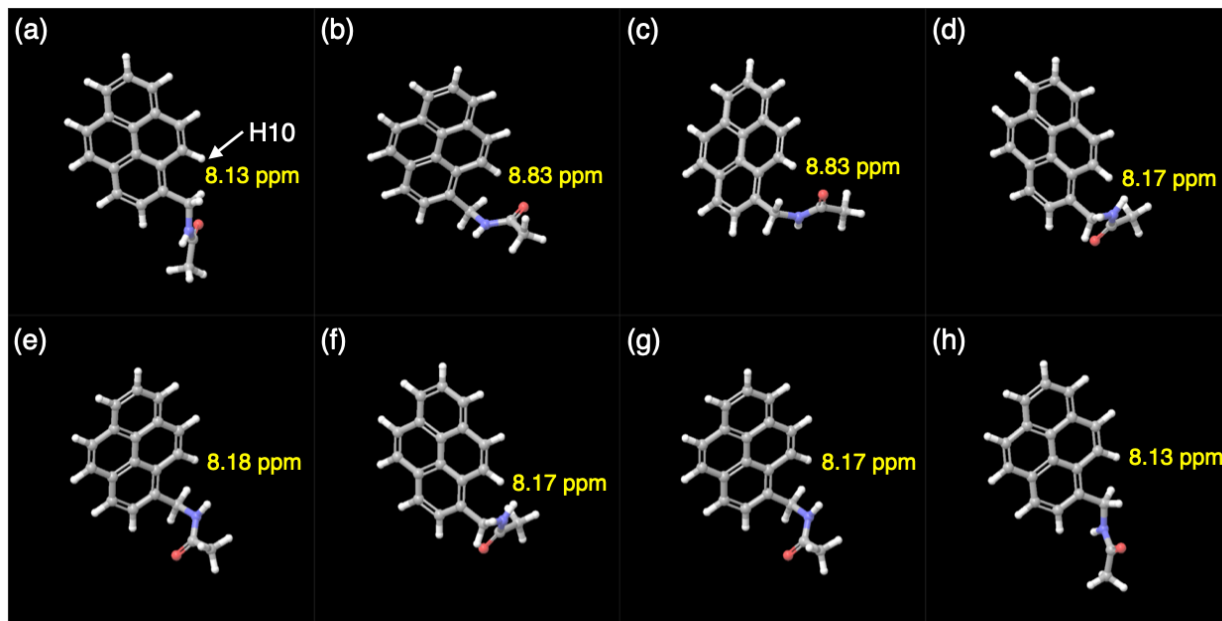


Figure S8. Density functional theory (DFT)-based proton NMR prediction of *N*-(1-pyrenylmethyl)acetamide. Conformer in (b), (c) showed that H10 of pyrene was located adjacent to the oxygen of the amide bond, increasing chemical shift (or move to downfield).

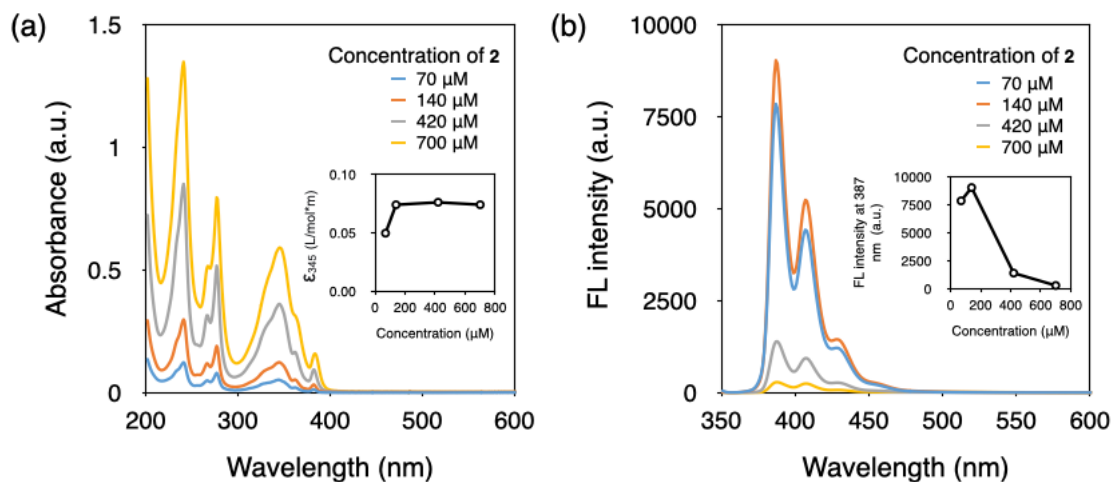


Figure S9. (a) Absorption and (b) emission spectra of molecule **2** at different concentrations (insets are the absorption coefficient and fluorescence intensity of **2** at 345 nm and 387 nm, respectively).

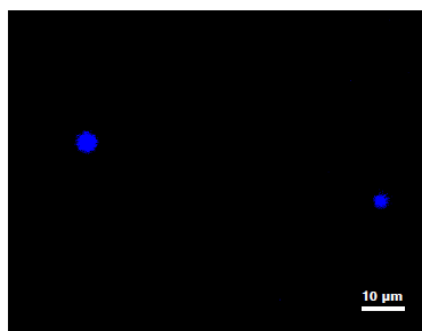


Figure S10. Spherical structures of molecule **2** (140 μM) in aqueous solution was observed by fluorescence optical microscopy (FOM) using excitation filter at $\lambda_{\text{ex}} = 340\text{--}380$ nm and emission filter at $\lambda_{\text{em}} > 425$ nm.

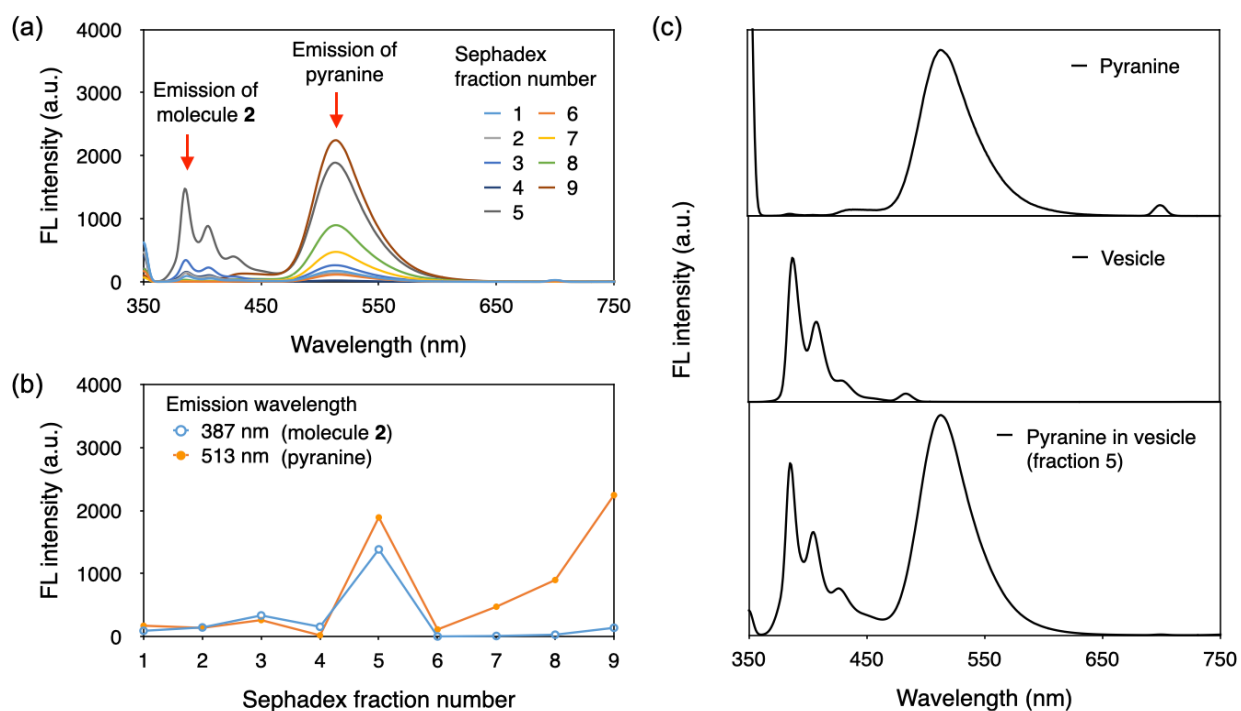


Figure S11. The encapsulation of pyranine into the vesicles was confirmed after separation of the untrapped molecules by GPC using sephadex column. (a) Fluorescence spectra and (b) intensity of fractions collected by sephadex column. (c) Emission spectrum of fraction 5 showed both peaks corresponding to the vesicles of **2** and the pyranine dye (all fractions were excited at 347 nm).

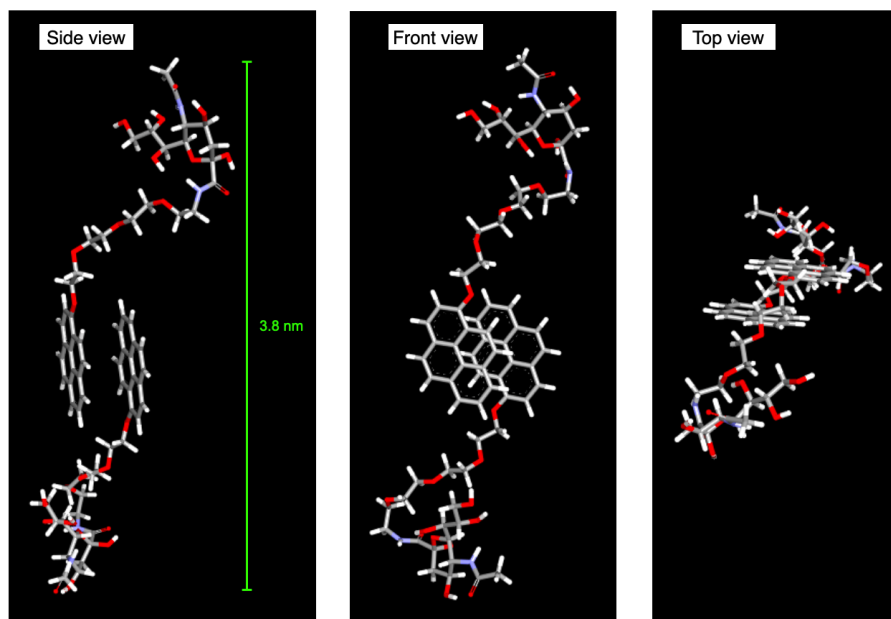


Figure S12. Molecular simulation of dimer **2**. The length was measured after energy minimization via DFT calculation.

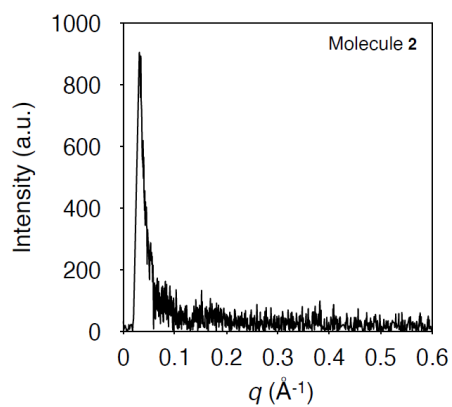


Figure S13. Small-angle X-ray scattering (SAXS) spectrum of molecule **2**.

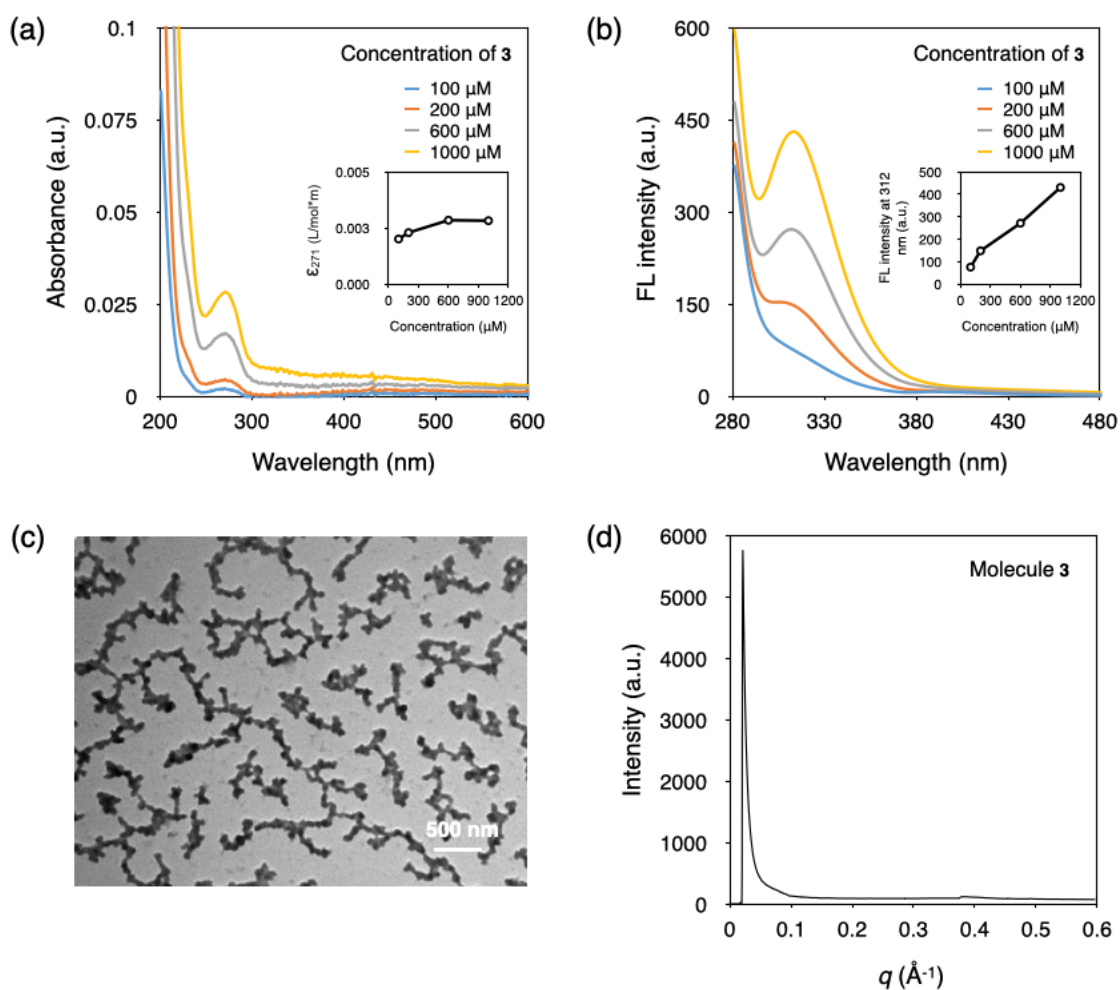


Figure S14. Self-assembled structure of amphiphile **3** in aqueous solution. (a) Absorption and (b) emission spectra of molecule **3** at different concentrations (insets are the absorbance and fluorescence intensity of **3** at 271 nm and 312 nm, respectively). (c) Transmission electron microscopy image of irregular aggregates of **3**. (d) SAXS spectrum of amphiphile **3**.

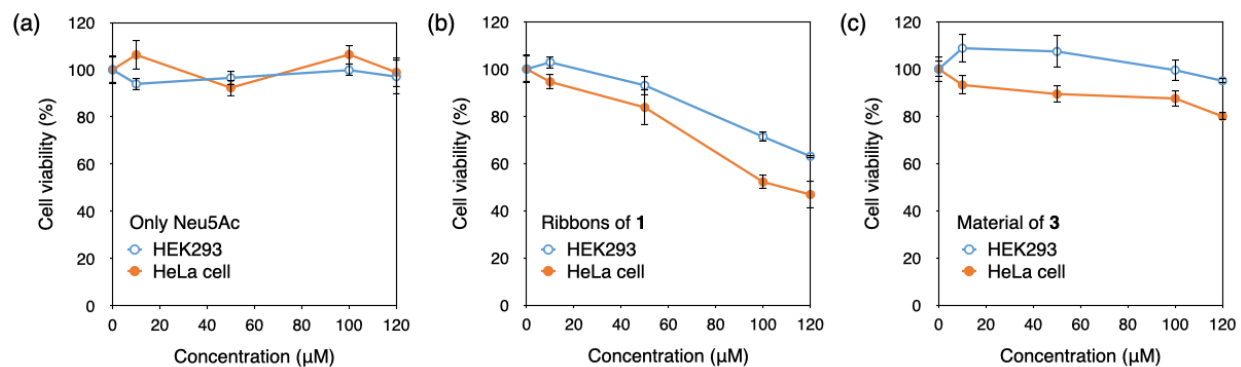


Figure S15. Cell viability of HeLa and HEK293 cells incubated with (a) only *N*-acetylneuraminic acid (Neu5Ac), (b) ribbons of **1**, and (c) material of **3** measured by MTT assay. The three materials did not show considerable selectivity between HeLa and HEK293 cells ($n = 5$).

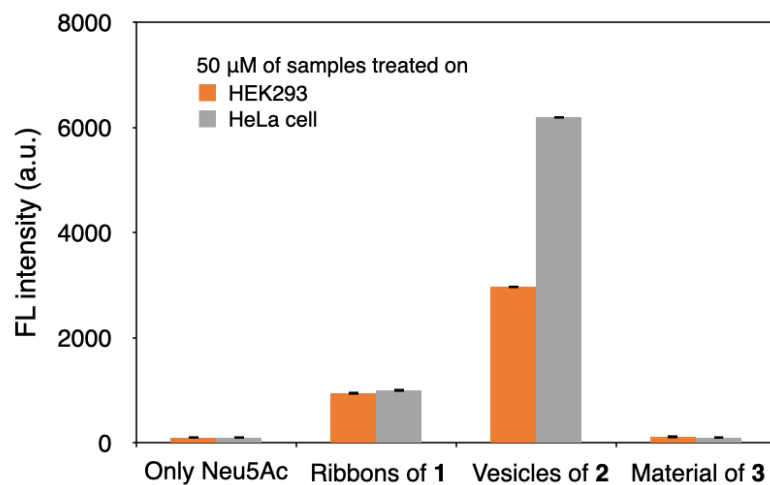


Figure S16. Fluorescence intensity of HeLa and HEK293 cells incubated with only Neu5Ac or materials of **1**, **2**, and **3** measured by cell imaging multi-mode reader (cytation) at 400 nm.

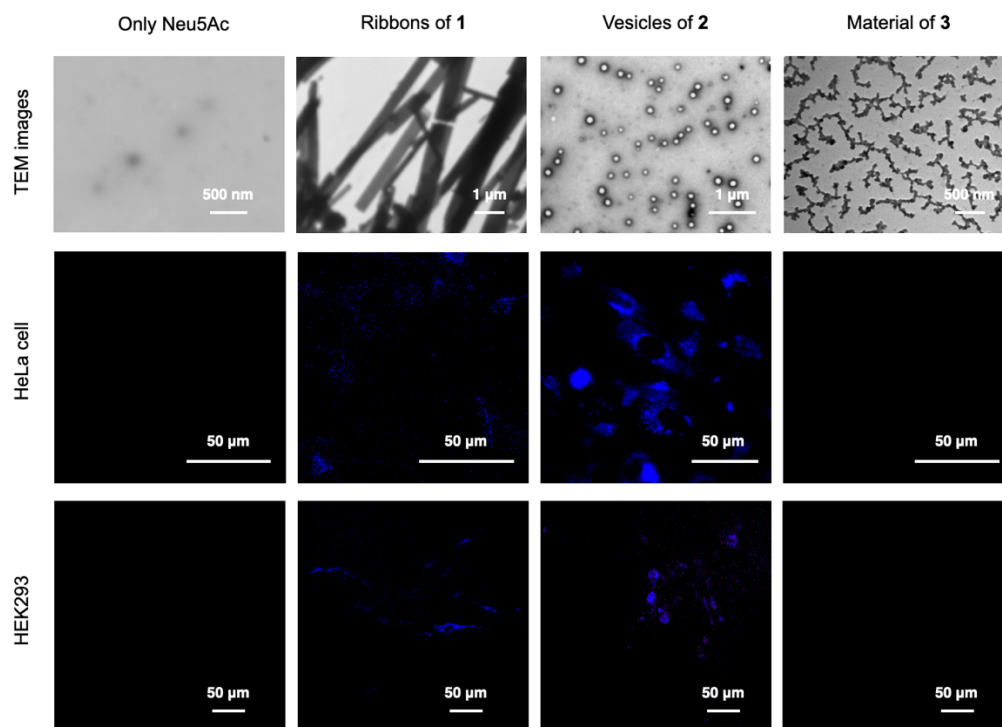


Figure S17. TEM images of only Neu5Ac or materials of **1**, **2**, and **3** and FOM images of those incubated with HeLa and HEK293 cells. Material **2** on HeLa cells showed the highest fluorescence indicating the highest uptake (scale bar, 50 μm). Fluorescence of pyrene was observed by excitation filter at $\lambda_{\text{ex}} = 340\text{--}380$ nm and emission filter at $\lambda_{\text{em}} > 425$ nm.

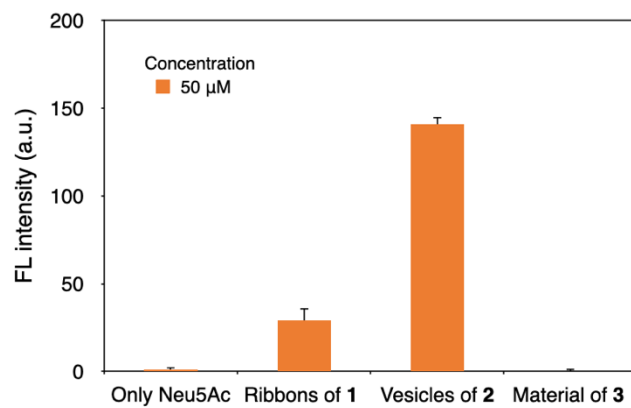


Figure S18. Fluorescence intensity of DCFDA-dyed HeLa cells with only Neu5Ac or materials of **1**, **2**, and **3** at 50 μM measured by FOM images.

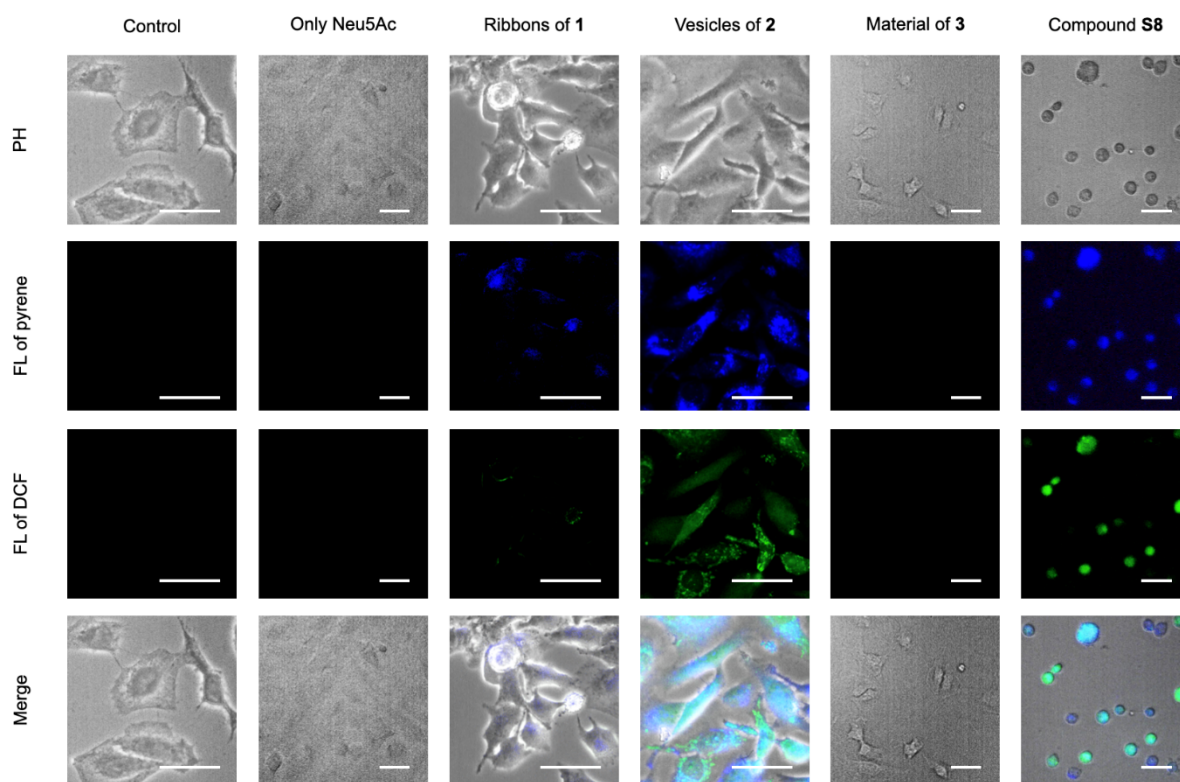


Figure S19. FOM images of HeLa cell dyed with DCFDA after incubation with only Neu5Ac, compound **S8** and materials of **1**, **2**, and **3** to confirm the amount of intracellular ROS generated by pyrene group. Material **2** showed the highest fluorescence indicating the highest ROS generation (scale bar, 50 μm).

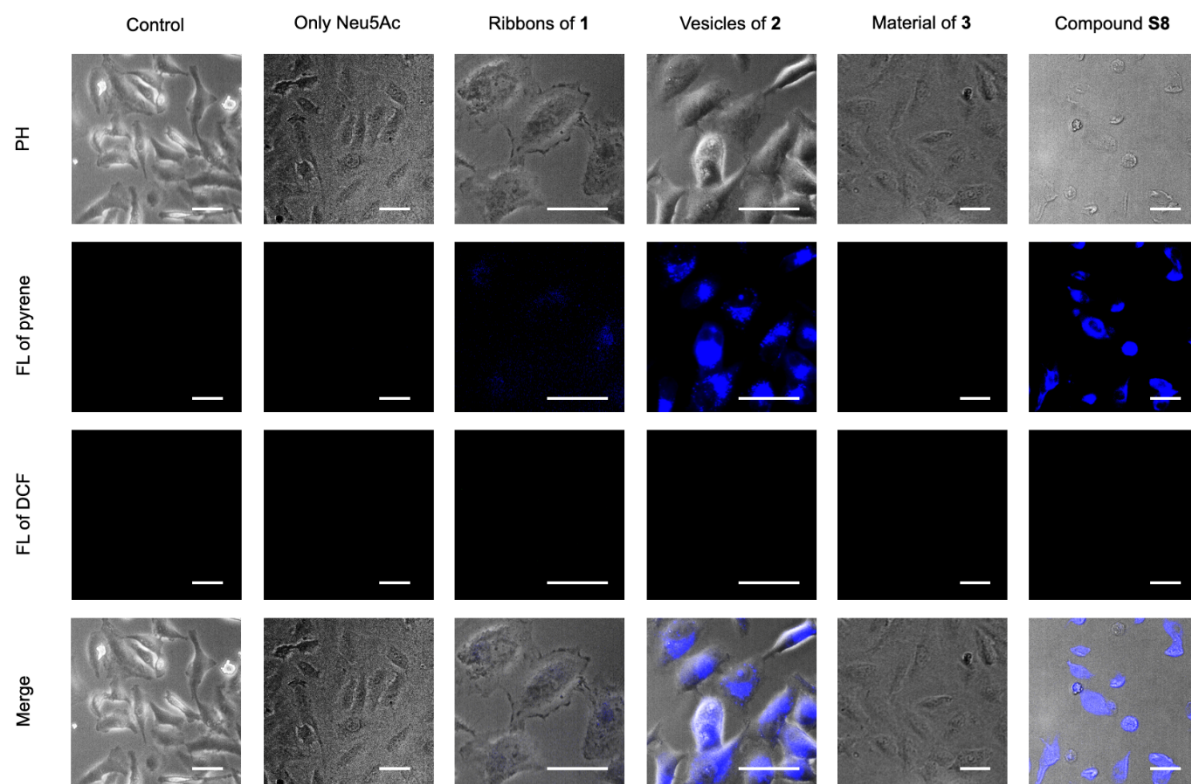


Figure S20. FOM images of HeLa cells without DCFDA after incubation with only Neu5Ac, compound **S8** and materials of **1**, **2**, and **3** (scale bar, 50 μm).